AIP | Journal of Applied Physics

Optical and magneto-optical study of nickel and cobalt ferrite epitaxial thin films and submicron structures

Cameliu Himcinschi, Ionela Vrejoiu, Georgeta Salvan, Michael Fronk, Andreas Talkenberger et al.

Citation: J. Appl. Phys. **113**, 084101 (2013); doi: 10.1063/1.4792749
View online: http://dx.doi.org/10.1063/1.4792749
View Table of Contents: http://jap.aip.org/resource/1/JAPIAU/v113/i8
Published by the American Institute of Physics.

JOURNAL OF APPLIED PHYSICS **113**, 084101 (2013)

Optical and magneto-optical study of nickel and cobalt ferrite epitaxial thin films and submicron structures

Cameliu Himcinschi,[1,a)] Ionela Vrejoiu,[2,b)] Georgeta Salvan,[3] Michael Fronk,[3] Andreas Talkenberger,[1] Dietrich R. T. Zahn,[3] David Rafaja,[4] and Jens Kortus[1]
[1]*TU Bergakademie Freiberg, Institute of Theoretical Physics, D-09596 Freiberg, Germany*
[2]*Max Planck Institute of Microstructure Physics, Weinberg 2, D-06120 Halle, Germany*
[3]*TU Chemnitz, Semiconductor Physics, D-09107 Chemnitz, Germany*
[4]*TU Bergakademie Freiberg, Institute of Materials Science, D-09596 Freiberg, Germany*

(Received 6 December 2012; accepted 6 February 2013; published online 22 February 2013)

Epitaxial films and ordered arrays of submicron structures of nickel and cobalt ferrites were deposited on Nb doped $SrTiO_3$ by pulsed laser deposition. X-Ray diffraction and atomic force microscopy showed that the films have a good crystalline quality and smooth surfaces. A larger number of phonon bands was observed in the polarization dependent Raman spectra of the ferrite films than expected for the cubic spinel structures. This is explained by short range ordering of the Ni^{2+} (or Co^{2+}) and Fe^{3+} cations at the octahedral sites inducing a lowering of the symmetry. The same behavior was also observed in the Raman spectra measured for the submicron structures, suggesting the same cation distribution as in the films. The diagonal components of the dielectric function for nickel and cobalt ferrites are determined from ellipsometry in the 0.73–5 eV photon energy range. The absorption edge was analyzed using a bandgap model and the energies for the indirect and direct optical transitions were calculated. It was found that both nickel and cobalt ferrites are indirect bandgap materials with bandgaps of 1.65 eV and 1.42 eV, respectively, while the first direct transitions lie at 2.69 eV and 1.95 eV, respectively. Magneto-optical Kerr effect spectroscopy in combination with spectroscopic ellipsometry allowed the off-diagonal elements of the dielectric tensor to be determined in the energy range from 1.7 eV to 5 eV. © *2013 American Institute of Physics*. [http://dx.doi.org/10.1063/1.4792749]

INTRODUCTION

$CoFe_2O_4$ (CFO) and $NiFe_2O_4$ (NFO) are insulating ferrimagnetic spinel oxides that are attractive for magnetoelectric oxide heterostructure devices, as well as various types of high frequency and high power applications.[1,2] MFe_2O_4 (M = Co or Ni) crystallizes in an inverse spinel structure with a general formula for the ion distribution $A^{3+}[B^{2+}B^{3+}]O_4^{2-}$ where A denotes tetrahedral cation sites and B denotes octahedral cation sites. The tetrahedral A-sites are occupied by half of the Fe^{3+} cations, while the octahedral B lattice sites are occupied by the rest of the Fe^{3+} cations and the divalent M^{2+} cations. Due to the occurrence of two types of magnetic ions at the octahedral sites, the two magnetic sublattices lead to a volume magnetization of 0.45 MA/m for CFO, and 0.33 MA/m for NFO.[3] A small fraction of the divalent cations can be found at the tetrahedral sites depending on the sample preparation or thermal history of the samples.[4–7]

Raman spectroscopy has been proven to be a sensitive tool to short-range site ordering of the cations in spinel ferrites. Polarized Raman spectra of single crystal NFO indicated a 1:1 ordering of Ni^{2+} and Fe^{3+} at B-sites, inducing a distortion of the structure to a tetragonal symmetry.[8] Pronounced B-sites ordering was also evidenced by Raman spectroscopy by Iliev *et al.*[9] in NFO thin films. Epitaxial strain was found to have an influence on the cation distribution in spinel ferrites.[10] The influence of hydrostatic strain on the spinel structure of polycrystalline CFO,[11] the response of epitaxial CFO thin films to biaxial compressive stress,[12] and the influence of heteroepitaxially induced strain in $BiFeO_3$-CFO nanostructures[13] were also studied using Raman spectroscopy.

While spectroscopic ellipsometry (SE) is commonly used to determine the optical constants and the optical bandgap of various materials, magneto-optical Kerr effect (MOKE) spectroscopy in combination with SE is often applied to obtain the off-diagonal dielectric tensor elements of oxides.[14,15] Numerous MOKE studies in various ferrites are reported in the literature and sometimes the interpretation of the electronic transitions observed in the spectra is contradictory (see, e.g., Fontjin *et al.*[16] for an overview). Only two reports exist on ferrite films, to the best of our knowledge. Kim *et al.*[17] reported MOKE spectra of Fe_3O_4, NFO, and CFO films with thicknesses of about 1 μm fabricated by sol gel. Mistrík *et al.*[18] reported MOKE spectra of a 93 nm thick NFO film deposited by pulsed layer deposition onto fused quartz substrates and found that the experimental spectrum was slightly shifted and broadened compared to the calculated one, probably due to structural defects.

Here the structural, optical, and magneto-optical properties of epitaxial CFO and NFO thin films are investigated by combining XRD, variable angle spectroscopic ellipsometry (VASE), MOKE, and Raman spectroscopy. In addition,

[a)]e-mail: himcinsc@physik.tu-freiberg.de.
[b)]Present address: Max Planck Institute for Solid State Research, 70569 Stuttgart, Germany.

arrays of submicron structures are also investigated by Raman spectroscopy.

EXPERIMENTAL

CFO and NFO epitaxial thin films were grown on Nb-doped $SrTiO_3$(100) (Nb:STO) substrates by pulsed-laser deposition (PLD), using stoichiometric ceramic targets. The films were deposited at a temperature of 575 °C in an oxygen pressure of 6×10^{-3} mbar. For the *in situ* PLD fabrication of ordered arrays of sub-micron CFO and NFO structures SiN stencil masks with rectangular apertures were used, as described elsewhere.[19] The structures were fabricated at the same temperature as the thin films, but in a lower oxygen pressure of 1.2×10^{-3} mbar.

The topography of the epitaxial CFO and NFO films and of the arrays of structures was investigated by atomic force microscopy (AFM) (Veeco, DI5000) working in tapping mode. The ellipsometric measurements were performed in the energy range from 0.73 eV to 5 eV at four angles of incidence using a M-2000 ellipsometer from J. A. Woollam Company. For the Raman scattering experiment, the samples were excited by the 532 nm line of a frequency doubled Nd:YAG laser and the spectra were collected by a LabRam spectrometer (Horiba Jobin Yvon) equipped with a Peltier cooled CCD detector and a 1800 grooves/mm grating. All spectra were obtained at room temperature in a backscattering geometry using an 100× magnification objective which focuses the laser to a spot size of about 1 μm. The laser power was set at 1 mW which was low enough in order to avoid damage of the samples surface and laser heating. The MOKE spectroscopic measurements were performed in polar geometry in the energy range from 1.7 eV to 5.5 eV using a home-built spectrometer based on the design from Herrmann *et al.*[20] The setup measures the rotation $\boldsymbol{\theta_K}$ and the ellipticity $\boldsymbol{\eta_K}$ of the polarization of the light reflected from the sample exposed to a magnetic field (1.7 T) perpendicular to the sample surface. These quantities correspond to the real and imaginary parts, respectively, of the complex Kerr rotation angle of the light polarization: $\Phi_k = \theta_k + i \cdot \eta_k$. The incidence angle is <1.3°. All measurements were carried out *ex situ* under ambient conditions and at room temperature. To exclude the contribution of optical anisotropy, the MOKE spectra were always recorded with the magnetic field pointing out from the sample and a second spectrum with the magnetic field pointing into the sample. The complex Kerr rotation spectra are then calculated as half the difference of the two spectra.

RESULTS AND DISCUSSIONS

In Figure 1(a), the θ-2θ XRD patterns of a ≈ 69 nm thick CFO film and of a ≈ 80 nm thick NFO film grown on Nb:STO substrates are shown. The graphs display the (004) reflection of the CFO and NFO films and the (002) reflection of the Nb:STO substrate. Cubic spinel $NiFe_2O_4$ has a bulk room temperature lattice parameter of a = 8.34 Å and $CoFe_2O_4$ has a = 8.39 Å. Hence a larger compressive lattice mismatch with the cubic perovskite Nb:STO substrate (a = 3.91 Å, which yields 2 a = 7.82 Å and thus a mismatch

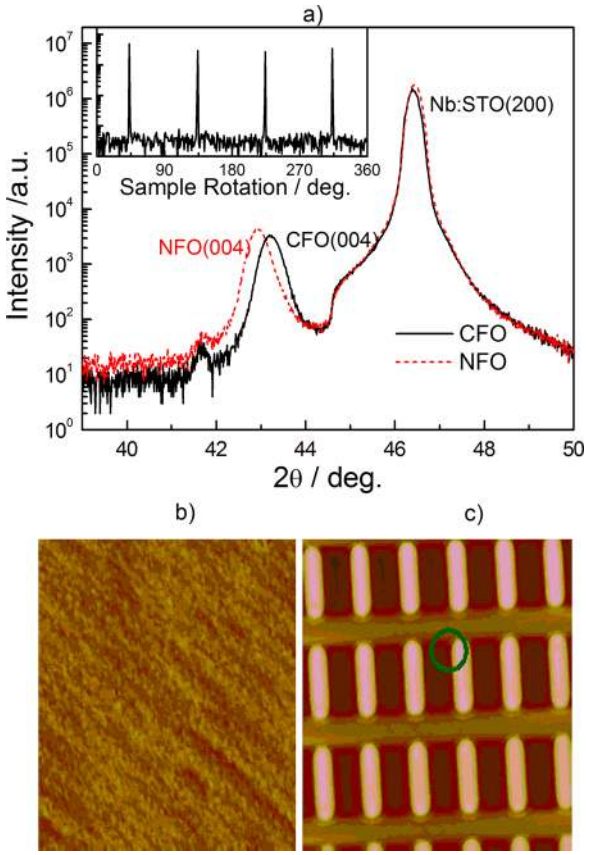

FIG. 1. θ-2θ XRD patterns of NFO and CFO films grown onto Nb:STO substrates. The inset shows a ϕ-scan of the NFO film taken at the sample inclination of 35.3°. (a) Tapping mode AFM image (4 μm × 4 μm, z-range = 1.5 nm) of a 80 nm thick CFO film deposited onto Nb:STO substrate. (b) AFM image (8 μm × 8 μm, z-range = 70 nm) of the CFO structures. The circle gives an estimation of the laser spot size in comparison to the structures dimensions. (c)

of 6.6% for bulk NFO and of 7.3% for bulk CFO with respect to the Nb:STO) is expected for the CFO film, leading to a shift of the 004 reflection peak towards lower angles. However, due to the very large mismatch, it is likely that the CFO film relaxes the strain by forming structural defects such as misfit dislocations at a smaller critical thickness than the NFO film. This may explain why the position at which the (004) reflection of the CFO film occurs is at a larger 2θ angle than the same reflection of the NFO film (Fig. 1(a)), indicating that the NFO film is much more strained and has a larger out-of-plane lattice parameter than the CFO film. The formation of other types of extended structural defects and of point defects such as oxygen vacancies may also contribute to the values of the lattice parameters of the films, which deviate from those of the bulk CFO and NFO. Still, the CFO and NFO films grew heteroepitaxially on the Nb:STO substrate. The heteroepitaxial growth was confirmed by the pole figure measurements that were measured on a Bragg-Brentano diffractometer. As a source of the X-rays, the Ni-filtered radiation of a Cu anode ($\lambda = 0.15418$ nm) was employed. The pole figures were measured as a sequence of ϕ-scans at different inclinations of the sample from its symmetrical position. Exemplarily, a single ϕ-scan taken at the sample inclination of 35.3° for the NFO film is shown in inset of Fig. 1(a).

The topography of the films and of their submicron-structures was investigated by AFM. Figures 1(b) and 1(c) show two typical AFM micrographs of the 69 nm thick CFO film and of CFO structures, respectively. The CFO and NFO films were relatively smooth, with rms roughness values below 1 nm for CFO/STO for the $4\,\mu m \times 4\,\mu m$ scanned areas. For the CFO submicron structures, an $8\,\mu m \times 8\,\mu m$ area was scanned. Figure 1(c) reveals arrays of ordered structures of uniform shape and size, having dimensions of about $1.8\,\mu m \times 0.5\,\mu m$. The z-range in Figure 1(c) is 70 nm. The circle gives an estimation of the laser spot size used for Raman mapping in comparison to the structure dimensions.

In Figure 2(a), the Raman spectra measured for a Nb:STO(100) substrate and for a 69 nm CFO film grown Nb:STO are shown. The spectra were normalized to the same intensity and the substrate spectrum was subtracted from the film/substrate spectrum. The obtained difference spectrum is shown in the lower part of the figure. The same normalization procedure was applied also for the spectra measured for NFO films and for the measurements performed in different polarization configurations. Removing the substrate contribution from the Raman signal of the ferrite films is important for a clear assignment of the peaks. The direct evaluation of the spectra of the film and substrate[21] can lead to ambiguous peak assignment because the Nb:STO substrate has peaks in the region where the ferrite films also reveal features, as can be see in Figure 2(a).

The spinel structure can be described by the space group $Fd\bar{3}m$ (No. 227) and factor group analysis predicts 5 Raman active internal modes: $A_{1g} + E_g + 3T_{2g}$.[8,22] The comparison of the polarized Raman spectra for NFO and CFO films deposited onto Nb:STO is shown in Figure 2(b). The spectra were measured in backscattering geometry in which the directions of the incident and scattered light are parallel with the normal to the films surface (z). In the parallel polarization configuration (y, y), the polarization directions for the incident and scattered light were both along a [001] direction of the cubic STO substrate, while for the cross polarization (x, y) the detection of the scattered light was realized in a polarization direction perpendicular to that of the incident light. The clear dependence of the Raman spectra on the polarization geometry suggests that the films are epitaxial. As can be seen in Figure 2(b), the number of the observed Raman lines exceeds the expected number of Raman peaks for the spinel structure. The spectra and the polarization dependence in Figure 2(b) for NFO films is very similar to those observed by Ivanov *et al.*[8] for NFO single crystals and by Iliev *et al.*[9] for NFO epitaxial films. This behavior was explained by a short range order of Ni^{2+} and Fe^{3+} cations which induces domain formation with lower symmetry than the cubic inverse spinel one ($Fd\bar{3}m$) and thus new sets of Raman modes. In the spectrum measured in parallel polarization configuration for the NFO films 7 peaks could be clearly identified at $\sim$ 338, 457, 493, 575, 596, 675, and 710 cm^{-1} while for the spinel structure only one A_{1g} and one E_g mode are expected. On the other hand, in the spectrum measured in cross polarization configuration peaks are observed at $\sim$490, 590, 670, and 703 cm^{-1}, instead of two F_{2g} modes which are expected for the spinel structure in our measured range. The positions of the bands and their dependence on polarization resemble those observed for NFO single crystals and NFO films deposited onto $MgAl_2O_4$.[9] Based on these similarities and the symmetry consideration which were discussed in detail by Ivanov *et al.*[8] the additional peaks seen in our spectra could be consistent with the ordering of Ni^{2+} and Fe^{3+} at the octahedral sites, which arises from a structure having tetragonal $P4_122/P44_322$ symmetry coexisting with an orthorhombic structure variant. A direct assignment of each single mode in our spectra cannot be realized because of the tetragonal and orthorhombic phase mixture and mainly because the epitaxial thin films do not allow the measurements in sufficient polarization configurations. A fully inverse octahedral B site arrangement which corresponds to tetragonal symmetry was also found to be

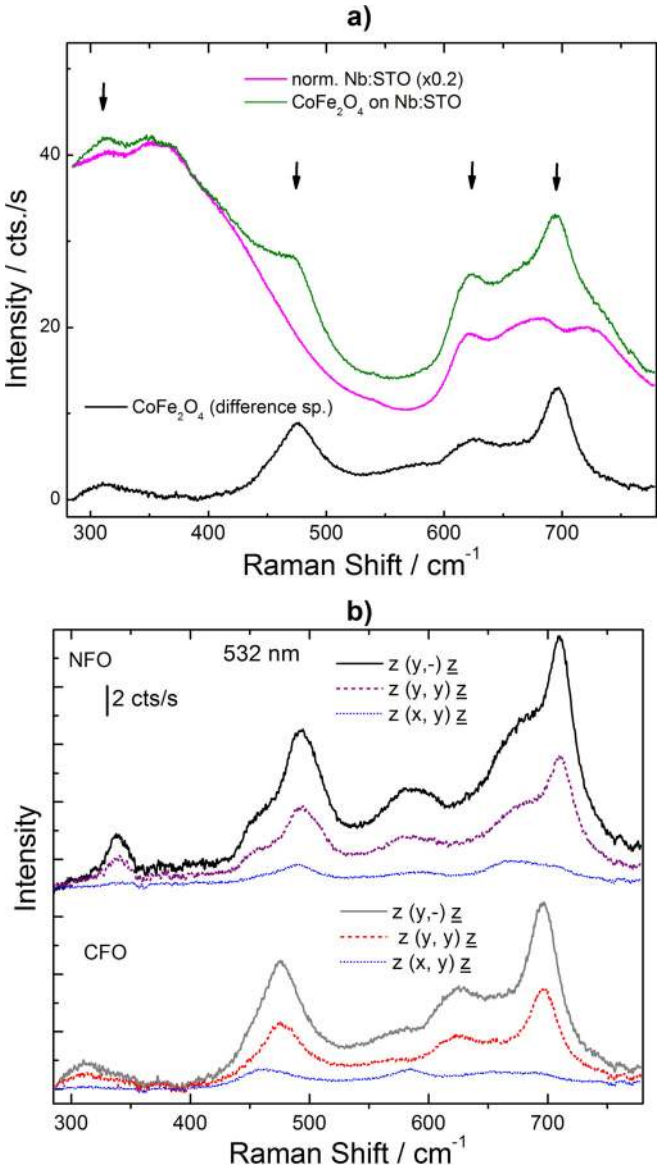

FIG. 2. Normalisation procedure: Raman spectra of Nb:STO substrate (scaled) and of a 80 nm CFO film deposited onto Nb:STO, measured with the 532 nm laser line. The arrows indicate the position of the strongest CFO phonon bands. The difference spectrum is shown in the lower part of the figure. (a) The Raman signal of the NFO (up) and CFO (down) films measured in different polarization configurations. (b)

energetically most favorable by using density functional theory[10] for both NFO and CFO materials. The spectra of the CFO films measured in different polarization configurations shown in the lower part of Figure 2(b) also show a larger number of phonon bands than expected for the ideal spinel structure. This behaviour was again attributed to the local short ordering of Co^{2+} and Fe^{3+} at the octahedral sites which induces the lowering of the symmetry.[12]

Raman measurements were also performed on the structured samples. The circle plotted in Figure 1(c) gives an indication of the laser spot size. Due to the dimension of the laser spot, the lateral resolution is low, thus each single Raman measurement contains contribution from both ferrite structures and the underlying and/or uncovered substrate. The Raman signal of the structures is obtained by performing the same normalization procedure as for the films. In Figures 3(a) and 3(b), typical Raman measured spectra are shown for the CFO and NFO structures, respectively, in comparison with the spectra of the films. As can be seen similar spectra were measured also for the structured arrays suggesting the preservation in the structures of the cation distribution at the tetragonal and octahedral sites as in the epitaxial thin films. This means that the deposition and stoichiometry of the submicron structures are not disturbed by the stencil mask. The small differences in the relative intensities could be explained by a partial relaxation of the epitaxial strain in the structures through the free surfaces of the structure edges.

In order to determine the dielectric function of the NFO and CFO films, the Nb:STO substrate was measured first by ellipsometry. The optical response of the substrate was described using a model consisting of Gaussian oscillators, which ensured the Kramer-Kronig consistency of the real and imaginary parts of the dielectric function. Using the dielectric function of the substrate, the ellipsometric spectra of the ferrite films were evaluated. The absorption free range, below 1.4 eV was used first for an initial estimation of the films thicknesses using a Cauchy dispersion relation for the refractive index. Further, the ellipsometric spectra were evaluated in the whole energy range employing a four-phase model: substrate/film/roughness layer/ambient. A sum of four Gaussian oscillators was used to simulate the optical response of the films, while the roughness layer was considered to be a mixture of 50% film material and 50% voids using Bruggeman effective medium approximation.[23] Thicknesses of 69.3 nm and 80.4 nm were obtained from the ellipsometric evaluation for the NFO and CFO films, respectively, the roughness being below 3 nm in both cases, in good agreement with the AFM results. The real and imaginary parts of the dielectric functions for CFO and NFO are shown in Figure 3(a). These diagonal components of the dielectric function were further used for the evaluation of the MOKE spectra. The dielectric function obtained for the CFO film is in good agreement with the one for a CFO crystal by Martens *et al.* which was determined above 1.5 eV.[15] Converting the dielectric function to optical constants a good agreement was also obtained with the optical constants of CFO and NFO crystals determined above 1.6 eV.[24] Our data extend the range of the dielectric functions down to 0.73 eV, which allows to use the absorption edge for optical gap

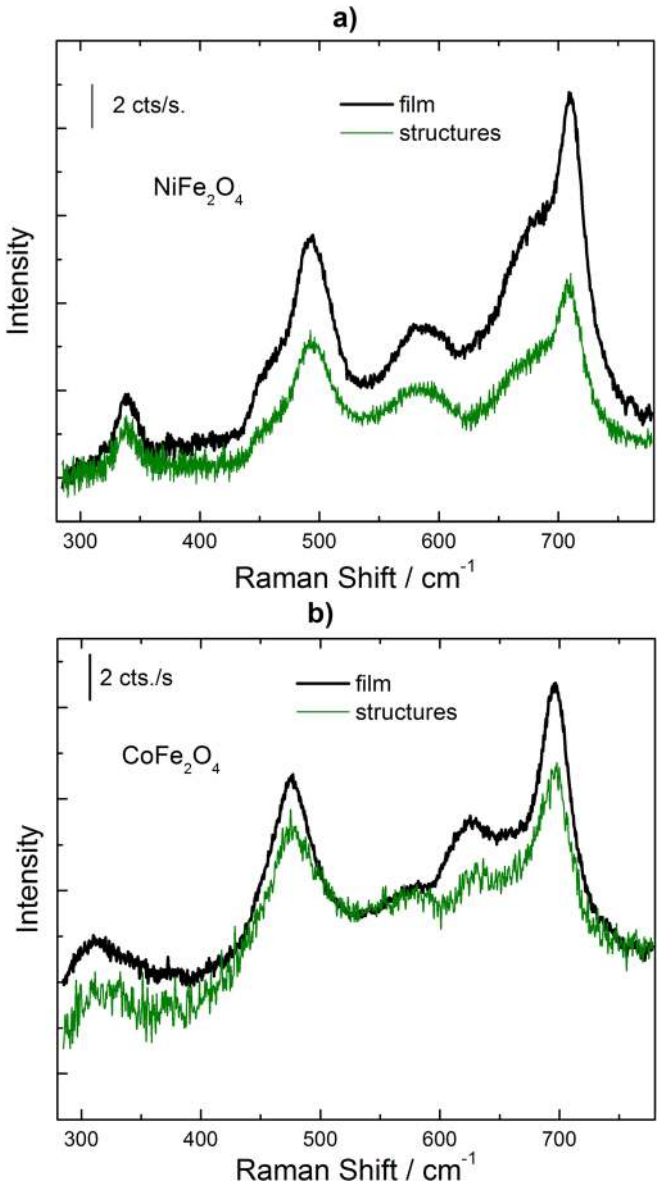

FIG. 3. Raman spectra of NFO (a) and CFO (b) thin films (continuous lines) and structures (dotted lines).

determination, as described below. It should be pointed out that the imaginary part of the diagonal component of the dielectric function is smaller for NFO than for CFO below 2.4 eV and larger above 3.5 eV. The involvement of possible transitions in this energy range will be discussed later in the evaluation of the magneto-optical data.

The energy and the type of transition for the optical gap of NFO and CFO films were determined by analyzing the absorption coefficient using the model proposed by Bardeen *et al.*[25] The absorption coefficient $\alpha = (4\pi k/\lambda)$ was calculated from the extinction coefficient k. The product of the absorption coefficient α and photon energy E is proportional to $(E - E_g)^{\eta}$, E_g is the energy of the optical bandgap, and the exponent η has a value of $1/2$ for direct transitions and a value of 2 for indirect transitions. In Figures 4(b) and 4(c), $(\alpha \cdot E)^{1/2}$ and $(\alpha \cdot E)^2$ were plotted versus photon energy for NFO and CFO, respectively. The linear extrapolation to zero absorption leads for NFO to values of 2.69 eV and 1.65 eV

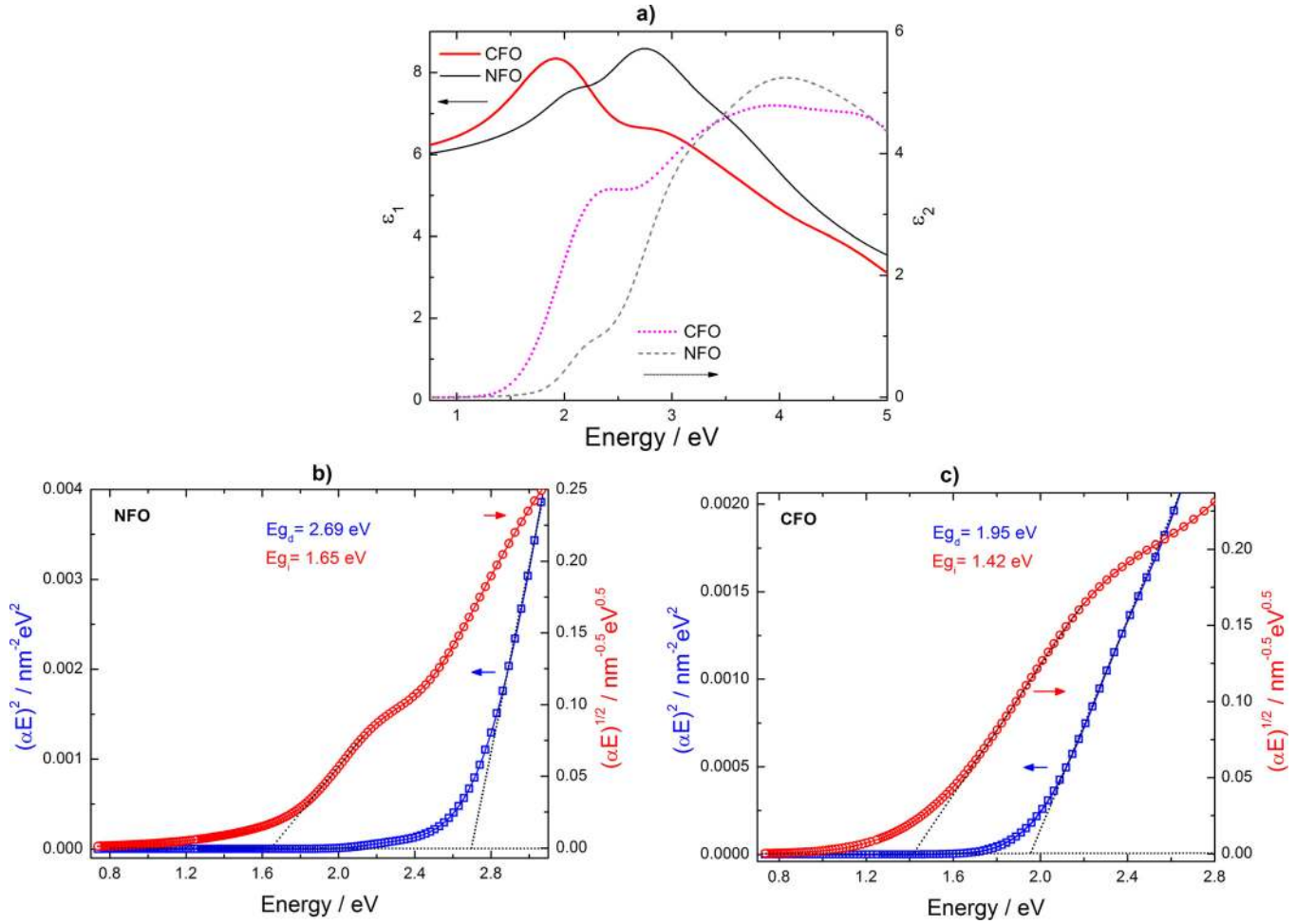

FIG. 4. Real (ε_1) and imaginary parts (ε_2) of the diagonal components of the dielectric function of NFO and CFO films deposited onto Nb:STO substrates as determined by evaluation of the ellipsometric data. (a) $(\alpha \cdot E)^2$ and $(\alpha \cdot E)^{1/2}$ plots as function of photon energy for NFO (b) and CFO (c) films. The linear extrapolations of $(\alpha \cdot E)^2$ and $(\alpha \cdot E)^{1/2}$ to zero give the values for optical band gaps of the direct and indirect transitions, respectively.

for the direct and indirect transitions, respectively. For CFO these values were determined to be 1.95 eV and 1.42 eV. The same method has been employed before for modeling the absorption edge for multiferroic materials.[26,27] The error in the determination of these values was estimated to be ± 0.03 eV. The characteristic S-shape of $(\alpha \cdot E)^{1/2}$ which presents two distinct slopes suggests the phonon involvement in the optical absorption process[28,29] indicating that NFO and CFO are indirect bandgap materials. The values for the indirect transitions are larger than the values calculated from first principles for both NFO and CFO.[10,30] On the other hand, the values are smaller than those recently experimentally determined using absorption measurements for NFO[31] and CFO[32] thin films. It should be pointed out that the optical constants obtained from ellipsometry are more reliable than those obtained directly from absorption measurements particularly near to the absorption edge.

The MOKE rotation and ellipticity spectra of the NFO and CFO films are shown in Figure 5. The NFO film exhibits a smaller MOKE signal and therefore the NFO spectra were multiplied by a factor of 3 for a better comparison.

The lineshape of the polar Kerr rotation of the NFO film is similar to that observed for the (111) face of a nickel ferrite single crystal[33] only slight shifts and small differences in the relative intensities of the spectral structures are noticeable. The same observation also holds for the CFO film as compared to the reported MOKE spectra of a $CoFe_2O_4$ (111) single crystal.[15] The similarity between the film and crystal spectra can easily be understood at higher energies considering that the penetration depth, estimated from the optical constants determined in this work, is lower than the film thickness for photon energies above 2.21 eV (CFO) and 2.84 eV (NFO).

However, in order to avoid possible interference effects in the low energy region of the spectra, the off-diagonal component of the dielectric tensor was obtained as described in the following.

The magneto-optical Kerr effect can be described by the occurrence of off-diagonal components of the macroscopic dielectric tensor. In the polar MOKE geometry, as used in this work, the light propagates along the z direction and hence parallel to the magnetic field direction. The dielectric tensor for a tetragonal crystal, such as proposed by Fritsch *et al.*[10] for the investigated systems, exposed to a magnetic field applied along the c direction (along the z-axis) has the following form:

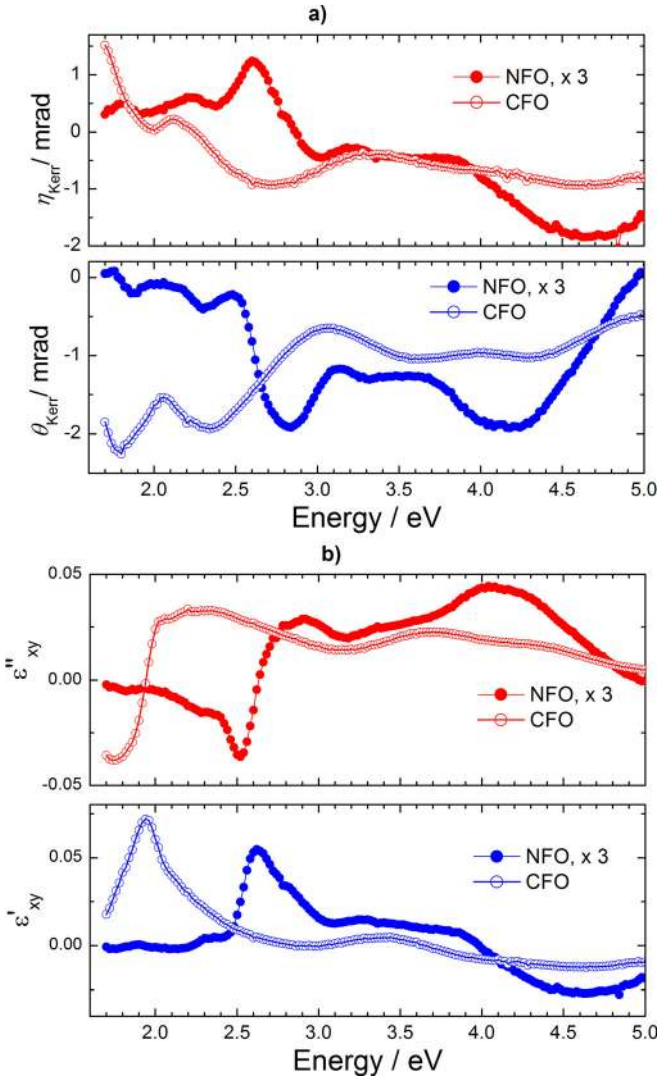

FIG. 5. Complex MOKE spectra of a 69 nm NFO film and of a 80 nm CFO film on STO substrates (a). Real (ε'_{xy}) and imaginary parts (ε''_{xy}) of the off-diagonal component of the dielectric tensor determined from the MOKE spectra and the diagonal components. (b)

$$\hat{\varepsilon} = \begin{bmatrix} \tilde{\varepsilon}_{xx} & \tilde{\varepsilon}_{xy} & 0 \\ \tilde{\varepsilon}_{xy} & \tilde{\varepsilon}_{xx} & 0 \\ 0 & 0 & \tilde{\varepsilon}_{zz} \end{bmatrix}, \quad (1)$$

where all tensor elements are complex quantities, i.e., $\tilde{\varepsilon}_{xx} = \tilde{\varepsilon}'_{xx} + i \cdot \tilde{\varepsilon}''_{xx}$ and $\tilde{\varepsilon}_{xx} = \tilde{\varepsilon}'_{xy} + i \cdot \tilde{\varepsilon}''_{xy}$. The off-diagonal component of the dielectric tensor can be expressed with the help of magneto-optical material constant Q, the so-called Voigt constant: $\tilde{\varepsilon}_{xy} = Q \cdot \tilde{\varepsilon}_{xx}$.[34]

For bulk samples, only the light reflected at the sample surface carries the magneto-optical information and the corresponding change in the light polarization upon reflection can be expressed in the following form:

$$\hat{\Phi}_K = \theta_K + i \cdot \eta_K = i \frac{\sqrt{\varepsilon_{xx}} Q}{1 - \varepsilon_{xx}}. \quad (2)$$

For a film with a thickness smaller than the penetration depth of the light, light can also be reflected at the interface film/substrate and the magneto-optical signal is influenced by interference effects. In this work, we will use the mathematical formalism from Fronk *et al.*[35] to extract the Voigt constant Q by a point-by-point fitting procedure from the MOKE spectra and from the optical constants obtained by spectroscopic ellipsometry. Thus, we calculated the off-diagonal elements of the dielectric tensor for comparison with reported values on ferrites (e.g., in Fontijn *et al.*[16]).

The STO substrate itself exhibits a small MOKE signal in the energy range between 4 eV and 5 eV. This was taken into account in the numerical calculation of the Voigt constant of the NFO and CFO films. The spectral dependence of the real (ε'_{xy}) and imaginary part (ε''_{xy}) of the off-diagonal component of the CFO dielectric tensor is shown in Figure 5(b). The shape and magnitude of the spectra are very similar to that reported for a CFO(111) single crystal.[15] The sign of ε'_{xy} is, however, inversed, due to different sign conventions used in the definition of the complex Kerr rotation angle. Only a few slight differences are noticeable: the transition between the crystal field (CF) splitted d orbitals of Co^{2+} is blue shifted in our case (by 0.12 eV); the intervalence charge transfer (IVCT) transition at ~2.2 eV is stronger in our films compared to the crystal, and the inter-sublattice charge transfer (ISCT) transition at ~4 eV is smaller in its relative intensity to the other bands compared to the crystal.[32] The observation of the CF band in mixed ferrites is attributed to a distortion of the octahedral site symmetry. Moreover, in ferrites with ions in the high spin state on the tetrahedral lattice sites (such as Co^{2+} in CFO) the CF transitions may have considerable oscillator strength.[16] The blue shift of the CF transition in our CFO film compared to the crystal might be related to the presence of residual strain in the films. The intensity decrease of the ISCT band at ~4 eV might be explained by a decrease in the net magnetic moment, probably due to structural defects reducing the symmetry of the octahedral and tetrahedral Fe^{3+} sites. A similar observation was reported for the NFO MOKE spectra of films compared to the bulk by Mistrik *et al.*[18]

In case of NFO, the ε'_{xy} and ε''_{xy} spectra calculated in this work exhibit sharper features compared to those reported for a NFO crystal in Ref. 36. This might be due to a better crystalline quality of the films compared to the crystals studied by Fontijn *et al.*[36] Our MOKE spectra are, however, well comparable to those of the 1 μm films studied by Kim *et al.*[17] We therefore refer to the latter reference for the assignment of the spectral features of films in this study.

The crystal field (CF) transition in NFO is much weaker compared to that in CFO, however, still detectable. For Ni^{2+} ions occupying octahedral sites the CF transitions are parity forbidden and should not be observed in NFO. However, if the film has a tetragonal symmetry as indicated by the Raman results, rather than a cubic symmetry, the parity selection rules for the Ni^{2+} ions at the octahedral sites are relaxed and the CF transitions can be observed. In addition, a small fraction (3.5% or less) of Ni^{2+} ions occupying tetrahedral sites could lead detectable MOKE signal[17] while hardly affecting the Raman spectra. The oscillator strength of the CF transition in NFO is lower than in CFO due to the lower spin state of the Ni^{2+} ($3d^8$) ions.

The energy of the transitions determined from the MOKE spectra and from the off-diagonal components of the

TABLE I. The energy of the transitions determined from the MOKE spectra and from the off-diagonal components of the dielectric tensor compared to the values reported for the 1 μm thick films and for the single crystals, respectively, along with the assignment of the spectral features. The ions situated at octahedral positions are denoted by square brackets and the tetrahedral sites are denoted by parentheses.

Sample	MOKE spectra energy/eV, This work	MOKE spectra energy /eV Sol-gel films, Ref. 17	ε'_{xy} spectra energy /eV, This work	ε'_{xy} spectra energy /eV Crystal, Ref. 16	Type	Transition assignment according to Kim *et al.*[17] assuming a cubic inversed spinel structure
CFO	1.78	2.0	1.94	1.82	CF(Co^{2+})	$^4A_2(^4F)\rightarrow{}^4T_1(P)$
	2.05	2.2	2.28	2.21	IVCT	$[Co^{2+}]t_{2g}\rightarrow[Fe^{3+}]t_{2g}$
	2.67	2.6	2.7	2.60	ISCT	$(Fe^{3+})t_2\rightarrow[Fe^{3+}]t_{2g}$
	3.6	3.6	3.68	3.55	IVCT	$[Co^{2+}]t_{2g}\rightarrow[Fe^{3+}]t_{2g}$
	4.3	4.0	4	4	ISCT	$(Fe^{3+})t_2\rightarrow[Fe^{3+}]e_g$
	4.7		4.6			
NFO	1.85	2.2	1.89		CF(Ni^{2+})	$^3T_1(^3F)\rightarrow{}^3A_2(F)$
	2.61	2.6	2.52	2.57	ISCT	$(Fe^{3+})t_2\rightarrow[Fe^{3+}]t_{2g}$
	3.1	3.1	3.15	2.86	IVCT	$[Ni^{2+}]t_{2g}\rightarrow[Fe^{3+}]t_{2g}$
	4.2	4.0	4.15	4.03	ISCT	$(Fe^{3+})t_2\rightarrow[Fe^{3+}]e_g$
	4.65	4.5	4.62		IVCT	$[Ni^{2+}]t_{2g}\rightarrow[Fe^{3+}]t_{2g}$

dielectric tensor (for comparison with Ref. 16) are summarized in Table I and compared to the values reported for the 1 μm thick films and for the single crystals along with the assignment of the spectral features. It should be noted that all band assignments proposed in the literature assume a cubic symmetry of the inverse spinel structure. A small tetragonal distortion should lead to a broadening of the bands compared to the real cubic structure.

From the difference between the energies of the IVCT transitions involving Fe^{3+} ions, the energy splitting between the t_{2g} and the e_g orbitals was calculated to amount to 1.4 eV for CFO and 1.47 eV for NFO. These values are consistent with that reported by Fontijn *et al.*[16]

SUMMARY

The Raman spectra measured on nickel and cobalt ferrite revealed a larger number of phonon bands than expected for the cubic spinel structure. Their polarisation dependence can be explained by a short range ordering of the divalent cations at the octahedral sites which induce a lowering of the symmetry, in agreement with the model proposed by Ivanov *et al.*[8] The Raman investigations performed on the ordered arrays of submicron structures showed the preservation of the cation distribution at the tetragonal and octahedral sites as in the corresponding epitaxial films. The dielectric function of the ferrite films was determined in the 0.73–5 eV energy range. A bandgap model was used to analyze the absorption edges and the energies of the first indirect and direct optical transition were determined for both cobalt and nickel ferrites. It was found that both materials have an indirect bandgap, with values of 1.65 eV and 1.42 eV for nickel ferrite and cobalt ferrite, respectively.

The off-diagonal components of the dielectric tensor determined from the MOKE spectra and ellipsometry spectra compare well with the reported bulk spectra for CFO, except slightly different relative intensities of the IVCT and ISCT bands, which might be related to the presence of structural defects that reduce the symmetry of the octahedral and tetrahedral Fe^{3+} sites in our films. The ε'_{xy} and ε''_{xy} spectra calculated in this work exhibit sharper features as compared to the bulk spectra reported by Fontijn *et al.*,[36] possibly due to a higher crystalline quality of the films.

ACKNOWLEDGMENTS

This work was supported by the German Research Foundation DFG HI 1534/1-1.

[1]N. Li, Y. H. A. Wang, M. N. Iliev, T. M. Klein, and A. Gupta, Chem. Vap. Deposition **17**, 261 (2011).
[2]Z. Chen and V. G. Harris, J. Appl. Phys. **112**, 081101 (2012).
[3]J. M. D. Coey, *Magnetism and Magnetic Materials* (Cambridge University Press, 2009).
[4]G. A. Sawatsky, F. van der Woude, and A. H. Morrish, Phys. Rev. **187**, 747 (1969).
[5]H. L. Yakel, J. Phys. Chem. Solids **41**, 1097 (1980).
[6]D. S. Erickson and T. O. Mason, J. Solid State Chem. **59**, 42 (1985).
[7]P. Chandramohan, M. P. Srinivasan, S. Velmurugan, and S. V. Narasimhan, J. Solid State Chem. **184**, 89 (2011).
[8]V. G. Ivanov, M. V. Abrashev, M. N. Iliev, M. M. Gospodinov, J. Meen, and M. I. Aroyo, Phys. Rev. B **82**, 024104 (2010).
[9]M. N. Iliev, D. Mazumdar, J. X. Ma, A. Gupta, F. Rigato, and J. Fontcuberta, Phys. Rev. B **83**, 014108 (2011).
[10]D. Fritsch and C. Ederer, Appl. Phys. Lett. **99**, 081916 (2011).
[11]Z. Wang, R. T. Downs, V. Pischedda, R. Shetty, S. K. Saxena, C. S. Zha, Y. S. Zhao, D. Schiferl, and A. Waskowska, Phys. Rev. B **68**, 094101 (2003).
[12]M. Foerster, M. Iliev, N. Dix, X. Marti, M. Barchuk, F. Sanchez, and J. Fontcuberta, Adv. Func. Mater. **22**, 4344 (2012).
[13]O. Chaix-Pluchery, C. Cochard, P. Jadhav, J. Kreisel, N. Dix, F. Sanchez, and J. Fontcuberta, Appl. Phys. Lett. **99**, 072901 (2011).
[14]W. F. J. Fontijn, P. J. van der Zaag, M. A. C. Devillers, V. A. M. Brabers, and R. Metselaar, Phys. Rev. B. **56**, 5432 (1997).
[15]J. W. D. Martens, W. L. Peeters, and H. M. Van Noort, J. Phys. Chem. Solids **46**, 411 (1985).
[16]W. F. J. Fontijn, P. J. van der Zaag, L. F. Feiner, R. Metselaar, and M. A. C. Devillers, J. Appl. Phys. **85**, 5100 (1999).
[17]K. J. Kim, H. S. Lee, M. H. Lee, and S. H. Lee, J. Appl. Phys. **91**, 9974 (2002).
[18]J. Mistrík, R. Lopušník, Š. Višňovský, N. Keller, M. Guyot, and R. Krishnan, J. Magn. Magn. Mater. **226–230**, 1820 (2001).
[19]I. Vrejoiu, A. Morelli, D. Biggemann, and E. Pippel, Nanoreviews **2**, 7364 (2011).
[20]T. Herrmann, K. Lüdge, W. Richter, K. G. Georgarakis, P. Poulopoulos, R. Nünthel, J. Lindner, M. Wahl, and N. Esser, Phys. Rev. B **73**, 134408 (2006).

[21]Y. Y. Liao, Y. W. Li, Z. G. Hu, and J. H. Chu, Appl. Phys. Lett. **100**, 071905 (2012).
[22]P. R. Graves, C. Johnston, and J. J. Campaniello, Mater. Res. Bull. **23**, 1651 (1988).
[23]D. E. Aspnes, J. B. Theeten, and F. Hottier, Phys. Rev. B **20**, 3292 (1979).
[24]G. S. Krinchik, K. M. Mukimov, Sh. M. Sharipov, A. P. Khrebtov, and E. M. Speranskaya, Zh. Eksp. Teor. Fiz. **76**, 2126 (1979).
[25]J. Bardeen, F. Blatt, and L. H. Hall, in *Photoconductivity Conference*, edited by R. G. Breckenridge, B. R. Russel, and E. E. Hahn (Wiley-Interscience, New York, 1956).
[26]C. Himcinschi, I. Vrejoiu, M. Friedrich, E. Nikulina, L. Ding, C. Cobet, N. Esser, M. Alexe, D. Rafaja, and D. R. T. Zahn, J. Appl. Phys. **107**, 123524 (2010).
[27]C. Himcinschi, I. Vrejoiu, T. Weißbach, K. Vijayanandhini, A. Talkenberger, C. Röder, S. Bahmann, D. R. T. Zahn, A. A. Belik, D. Rafaja, and J. Kortus, J. Appl. Phys. **110**, 073501 (2011).
[28]S. Guo, H. Arwin, S. N. Jacobsen, K. Järrendhal, and U. Helmersson, J. Appl. Phys. **77**, 5369 (1995).
[29]J. I. Pankove, *Optical Processes in Semiconductors* (Prentice-Hall, Englewood Cliffs, 1971).
[30]Z. Szotek, W. M. Temmerman, D. Ködderitzsch, A. Svane, L. Petit, and H. Winter, Phys. Rev. B **74**, 174431 (2006).
[31]R. C. Rai, S. Wilser, M. Gruminiak, B. Cai, and M. L. Nakarmi, Appl. Phys. A **106**, 207 (2012).
[32]A. V. Ravindra, P. Padhan, and W. Prellier, Appl. Phys. Lett. **101**, 161902 (2012).
[33]F. J. Kahn, S. P. Pershan, and J. P. Remeika, Phys. Rev. **186**, 891 (1969).
[34]J. Zak, E. R. Moog, C. Liu, and S. D. Bader, Phys. Rev. B **43**, 6423 (1991).
[35]M. Fronk, B. Bräuer, J. Kortus, O. G. Schmidt, D. R. T. Zahn, and G. Salvan, Phys. Rev. B **79**, 235305 (2009).
[36]W. F. J. Fontijn, P. J. van der Zaag, and R. Metselaar, J. Appl. Phys. **83**, 6765 (1998).